Thin-Walled Structures 187 (2023) 110739

Contents lists available at ScienceDirect

Thin-Walled Structures

journal homepage: www.elsevier.com/locate/tws

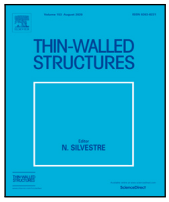

Full length article

Design of isotropic 2D chiral metamaterials based on monohedral pentagonal tessellations

Luke Mizzi [a,*], Luigi Grasselli [a], Andrea Spaggiari [a], Ruben Gatt [b,c], Pierre-Sandre Farrugia [b,d], Joseph N. Grima [b,e]

[a] Department of Sciences and Methods for Engineering, University of Modena and Reggio Emilia, Reggio Emilia, Italy
[b] Metamaterials Unit, University of Malta, Msida, Malta
[c] Centre for Molecular Medicine and Biobanking, University of Malta, Msida, Malta
[d] Department of Geosciences, University of Malta, Msida, Malta
[e] Department of Chemistry, University of Malta, Msida, Malta

ARTICLE INFO

Keywords:
Chiral honeycombs
Auxetic metamaterials
Monohedral pentagonal tessellations
Mechanical properties
Poisson's ratio

ABSTRACT

A novel class of transversely-isotropic metamaterials with the potential to exhibit a wide range of Poisson's ratios and stiffnesses is proposed in this work. These metamaterials, which also have the potential to exhibit auxetic behaviour, are formed through the chiralisation of 2D monohedral Euclidean pentagonal tessellations. Through Finite Element simulations and experimental testing on additively manufactured prototypes, we show that these systems can exhibit Poisson's ratios which encompass the entire range of transverse isotropicity, i.e. +1 to -1, and that the mechanical properties of these structures can be tailored considerably through variation of the geometric parameters without a loss of global symmetry and isotropy. The level of versatility observed in these new metamaterials exceeds by far that which is commonly found in traditional and well-known isotropic auxetic systems such as hexachiral honeycombs. In addition, analytical expressions pertaining to the geometric limits which define the realisability of this new class of auxetic metamaterials have also been derived and presented. The findings of this work demonstrate that pentagonal tessellations have considerable potential for the development of novel metamaterials and that the geometric constraints associated with transverse isotropy need not necessarily be an insurmountable barrier for the design of metamaterials with tailorable and versatile mechanical properties.

1. Introduction

Mechanical metamaterials have the ability to exhibit a myriad of anomalous and extraordinary characteristics due to the relationship between their structural framework and mechanical properties [1]. These unusual characteristics include 'negative' properties which are not commonly found in nature such as negative stiffness [2], compressibility [3], thermal expansion [4] and Poisson's ratio [5–7] (also known as auxeticity), which give rise to advanced functionalities making these materials/systems suitable for a variety of specialised applications. The latter type of systems, auxetic systems, are the most well-known class of mechanical metamaterials and various geometries which impart auxeticity have been established. These include re-entrant structures [8–11], rotating rigid unit systems [12–16], chiral honeycombs [17–36], origami/folding patterns [37,38], dilational [39] and helical systems [40], which have been reproduced and/or observed in sizes ranging from the macro- to the nanoscale.

Chiral honeycombs are a class of auxetic metamaterials which consist of chiral nodes that are attached to each other through ligaments. These systems are characterised by the presence of chirality, i.e. they have no axis of symmetry and the structure cannot be super-imposed on its corresponding mirror-image by rotations or translations alone in a 2D plane [41]. The first example of an auxetic chiral honeycomb found in literature is the hexachiral honeycomb. This auxetic system, first suggested in concept by Wojciechowski [42] and later implemented and realised in physical form by Prall and Lakes [18], is made up of circular nodes arranged at the vertices of an equilateral triangular tiling pattern, connected to each other through tangentially-attached slender ligaments (see Fig. 1a). Once subjected to uniaxial compressive or tensile loads, the system deforms predominantly through rotation of the circular nodes and flexure of ligaments exhibiting a Poisson's ratio of *ca.* −1. Aside from the hexachiral honeycomb [25,31,34,43–45], other chiral honeycombs have since been proposed based on quadrilateral and hexagonal tilings, namely the tetrachiral [31,34,43,44,46–48] and trichiral [31,34,49,50] honeycombs, respectively. These metamaterial structures have been shown to exhibit zero and negative Poisson's ratios, respectively. Furthermore, in addition

* Corresponding author.
E-mail address: luke.mizzi@unimore.it (L. Mizzi).

https://doi.org/10.1016/j.tws.2023.110739
Received 11 November 2022; Received in revised form 13 February 2023; Accepted 27 March 2023
Available online 5 April 2023

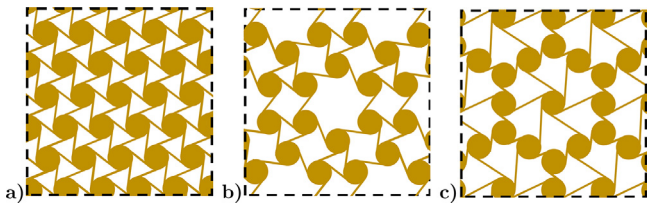

Fig. 1. (a) A regular hexachiral system based on a monohedral equilateral triangle tiling pattern. The chiral systems shown in (b) and (c), on the other hand, are based on a rhombi-trihexagonal and a deltoid-trihexagonal tessellation respectively. The former is an Archimedean tessellation consisting of equilateral triangles, squares and regular hexagons, while the latter is its corresponding dual structure. Similarly, to the hexachiral honeycomb, both these systems possess in-plane rotational symmetry of order 6 and, hence, exhibit transverse isotropy.

to these 'purely' chiral honeycombs, other variants have also been proposed which are made up of the same sub-units which are interconnected in a different arrangement to give rise to structures which possess an axis of symmetry. These systems, known as anti-chirals, also have the ability to exhibit a negative Poisson's ratio, with the most well-known forms being the anti-tetrachiral [51–57] and anti-trichiral [58,59] honeycombs. These forms have also inspired the design of further chiral and related metamaterials, including mixed or meta-chiral honeycombs [60,61], multi-polygonal motif-based systems [62–64], hierarchical chirals [28,32,65,66] and 3D-chiral honeycombs [67–70].

Auxetic metamaterials have been shown to exhibit a wide spectrum of Poisson's ratios, ranging from values close to zero down to giant negative values. Naturally, the latter property can only be obtained in specific loading directions from highly anisotropic systems, since the laws of structural continuum mechanics impose a strict limit on the absolute values of the Poisson's ratio which an isotropic material may possess, namely from +0.5 to −1. In the case of systems which exhibit only in-plane isotropy, or 'transverse isotropy' as it is more commonly known, this threshold is somewhat more negotiable and extends from +1 to −1 [71,72]. Systems exhibiting transverse isotropy are typically characterised by in-plane hexagonal symmetry and a number of metamaterial geometries exhibiting this property are known, with the prime example being the regular hexachiral honeycomb geometry (see Fig. 1a). As mentioned previously, the system possesses no line of axial symmetry and possesses hexagonal rotational symmetry.[1] Recently, other chiral metamaterials [62,63] have also been proposed, some of which also possess the same symmetry characteristics (and, hence, transverse isotropy) as well as the ability to exhibit auxetic behaviour, two examples of which are shown in Fig. 1b and c. These chiral systems were designed by the transformation (or 'chiralisation') of Euclidean polygonal tessellations and/or their dual counterparts into chiral metamaterials through the introduction of circular nodes at the vertices of the tilings connected together through tangentially-attached ligaments.

All of the structures shown in Fig. 1 and presented in previous works on chiral metamaterials exhibiting transverse isotropy, have one common factor – they are based on periodic tilings made from regular or highly symmetrical polygonal tessellations. This shared characteristic arises mainly from the fact that the mathematical laws which govern the design framework of tessellatable 2D geometries are very restrictive and permit a very limited range of monohedral (i.e. single polygon) tessellations with a global hexagonal symmetry based on asymmetric polygons. This has resulted in a situation where the symmetry of the system globally has never been investigated independently of the symmetry of the type of polygon constituting the tessellation itself, i.e. an asymmetric monohedral polygon-based tessellation which possesses hexagonal global rotational symmetry has not been considered previously with respect to its mechanical properties. According to the laws of structural mechanics, which consider only the global symmetry of the system, such a structure should exhibit transverse isotropy in spite of the irregularity of the constituent polygon shape – a factor which is highly unusual in the field of metamaterials, where irregularity is widely associated with anisotropy.

In this work we have designed a novel class of chiral metamaterials which possess this extremely unusual symmetry characteristic using pentagonal tilings. Grunbaum and Shephard [73] demonstrate in their book on tessellations a wide and distinct range of monohedral pentagonal tilings and establish the geometric conditions necessary to design said periodic tilings, including a class which exhibits a global rotational symmetry of order 6. This latter class of pentagonal tessellations forms the basis of this study and we show how, through the geometric variation of pentagonal design and extent of chiralisation, these new chiral metamaterial systems may be adapted to exhibit a wide range of mechanical properties whilst retaining their isotropic nature throughout – a characteristic which is unique to this particular topology.

2. Concept and design

In this section, we show how the monohedral pentagonal tessellation framework with hexagonal symmetry on which these chiral metamaterials are based may be constructed. In particular, the geometric conditions necessary for the formation of these systems are established as well as the limits which define whether the resultant tessellation is made up of concave or convex pentagons. This is then followed by a quantitative description of the chiralisation process used to transform these basic tessellations into chiral metamaterials.

2.1. Pentagonal tiling tessellations

Monohedral pentagonal tilings are a peculiar class of Euclidean polygonal tessellations. While it is commonly known that unlike triangles, squares and hexagons, it is impossible to create a space-filling tessellation made up solely from the regular variant of this polygon, pentagons show a high level of versatility and afford larger geometric variation when it comes to the design of monohedral tilings [73,74]. Indeed, for generic, irregular triangles and quadrilaterals one possible arrangement with a repeating unit possessing a rotational symmetry of order 2 exists which allows for the generation of space-filling monohedral structures, while in the case of convex hexagons only 3 forms are allowed. On the other hand, 13 distinct forms are permitted for pentagonal systems (listed in Grunbaum and Shephard's book [73]). In this study, we are interested in the one and only form in this list which gives a monohedral pentagonal tiling with a rotational symmetry of order 6 (classified as "Type 5 Pentagons" in [73]), an example of which is shown in Fig. 2a(i).

Although a wide range of pentagons can be used to generate this type of tessellation (i.e. with hexagonal rotational symmetry), they must conform to a strict set of geometric conditions in order to result in a periodic space-filling system. As indicated in Fig. 2a(ii), angles $B\hat{A}E$ and $B\hat{C}D$ must be equal to 60° and 120° respectively, while two pairs of sides: AE & AB and BC & CD must be equally sized. This means that the pentagonal units may be defined by three independent variables which define the three side lengths, hereby denoted by: i, j and k. The variable i defines the lengths of the sides AE & AB, j, the lengths of BC & CD and finally, k, the length of ED.

As shown in Fig. 2a(ii), the pentagons with vertices ABCDE considered in this study may be defined in terms of three triangles: ABE, BDE and BCD, where triangle BDE within the same Euclidean plane gives rise to the final pentagon of this family by simply building an external equilateral triangle ABE on the side BE and an external

[1] A figure, in particular a tiling, in the Euclidean plane has a rotational symmetry of order n if it is invariant under a $2\pi/n$ rotation centred in suitable points, the so-called rotation centres of order n. It is well-known that the only possible orders of n are 2, 3, 4 and 6.

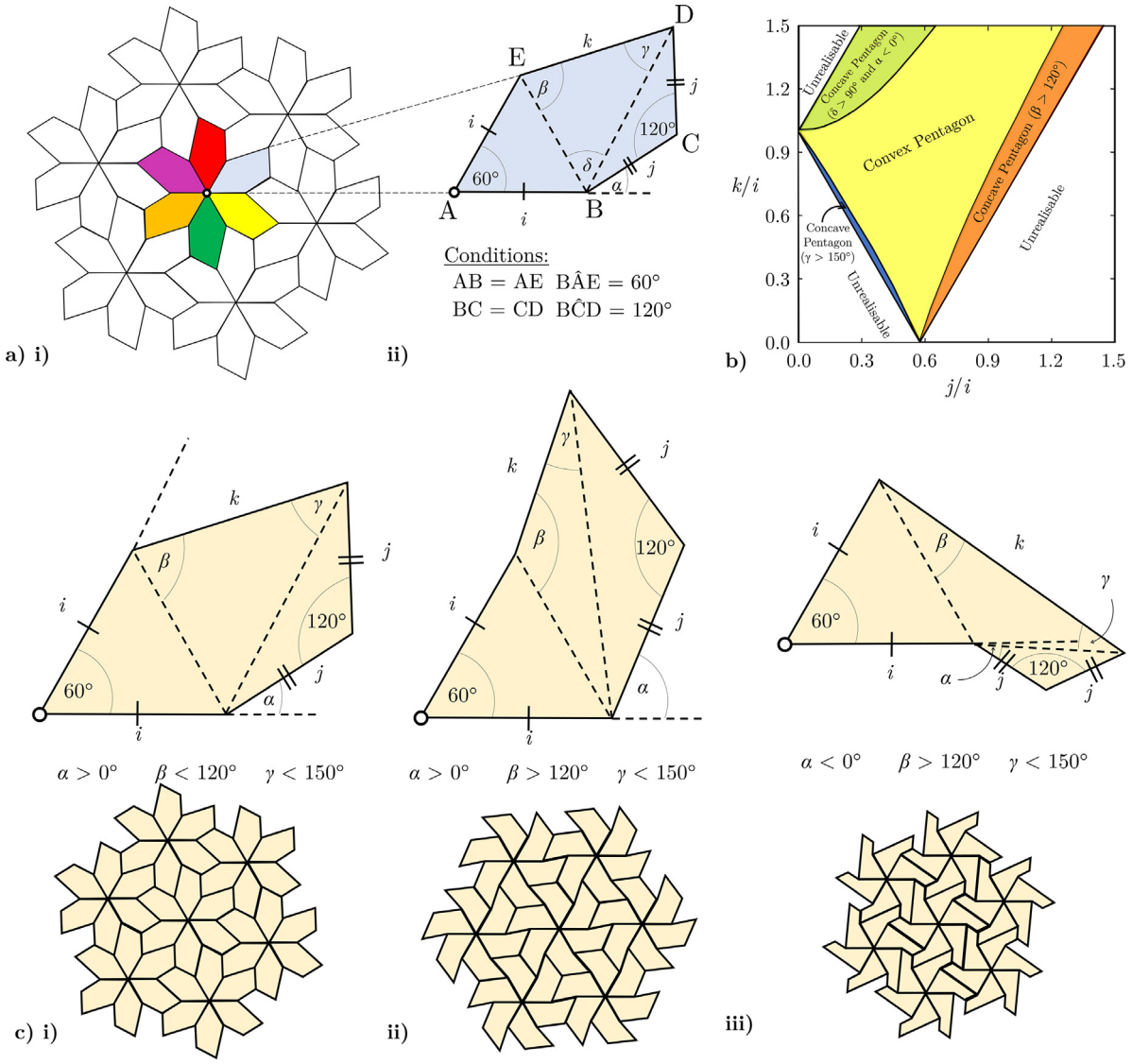

Fig. 2. (a) (i) An example of a monohedral pentagonal tessellation with hexagonal rotational symmetry made from irregular pentagons and (ii) a sketch indicating the geometric dimensions and conditions of the pentagon which must be satisfied in order to design this tessellatable space-filling system. (b) Plot showing how pentagon shape varies with changes to j/i and k/i ratios. The limits are plotted based on the equations presented in Appendix A. (c) Diagrams showing the geometric parameters used to define the pentagonal units and geometric conditions required to obtain (i) convex and (ii), (iii) concave pentagon-based monohedral tessellations with hexagonal rotational symmetry. The actual range of realisable structures with $\gamma > 150°$ is very small, as shown in (b), and therefore a representative figure is not shown.

isosceles triangle BCD, with base BD, such that $B\hat{C}D = 120°$. In other words, there is a one-to-one correspondence between the whole set of triangles in the Euclidean plane and the set of this particular type of pentagons. The length BD is always defined as $j\sqrt{3}$ and thus the sides of triangle BDE are of sizes: i, k and $j\sqrt{3}$. Therefore, the range of values for i, j and k which may be used to create pentagons pertaining to this family must satisfy the existence conditions for the triangle BDE, namely:

$$\begin{aligned} i + j\sqrt{3} &> k \\ j\sqrt{3} + k &> i \\ i + k &> j\sqrt{3} \end{aligned} \tag{1}$$

These conditions may also be expressed as a single equation (Eq. (2)). For any combination of values chosen for i, j and k, the following geometric condition must be adhered to:

$$\left| \frac{i^2 + 3j^2 - k^2}{2ij\sqrt{3}} \right| < 1 \tag{2}$$

As shown in Fig. 2c, it is possible to design a considerable spectrum of tessellatable structures from pentagons which satisfy these geometric requirements. This range incorporates systems which are based on both convex and concave pentagons. In order to obtain a convex pentagon (Fig. 2c(i)), the angles β, γ and δ must satisfy the following conditions: $\beta < 120°$, $\gamma < 150°$ and $\delta < 90°$, while a concave pentagon is designed if one of these conditions is not fulfilled (Fig. 2c(ii) and (iii)). The convexity condition relating to the internal angle δ may also be expressed in terms of the external angle α (see Fig. 2a(ii)) as follows: $\alpha > 0°$. The angles α, β, γ and δ may be calculated as a function of i, j and k (and by extension, of the quotients $\frac{j}{i}$ and $\frac{k}{i}$) as follows:

$$\alpha = \frac{\pi}{2} - \delta \tag{3}$$

$$\beta = \arccos\left[\frac{k^2 + i^2 - 3j^2}{2ik}\right] \tag{4}$$

$$\gamma = \arccos\left[\frac{k^2 - i^2 + 3j^2}{2jk\sqrt{3}}\right] \tag{5}$$

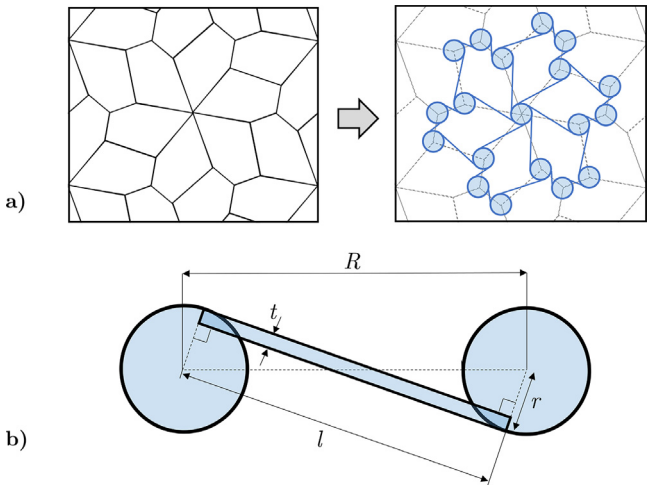

Fig. 3. (a) A schematic showing how chiral nodes are generated at the vertices of the original pentagonal tessellation and (b) a figure showing the geometric parameters used to define the chiralisation of these systems.

$$\delta = \arccos\left[\frac{i^2 - k^2 + 3j^2}{2ij\sqrt{3}}\right] \tag{6}$$

This means that the entire range of permissible pentagon relative dimensions which are realisable and whether they are convex or concave can be expressed as functions of the ratios $\frac{j}{i}$ and $\frac{k}{i}$, the results of which are plotted in Fig. 2b. The full equations pertaining to the existence and convexity conditions used to derive these plots are presented in more detail in Appendix A.

2.2. Chiralisation of pentagonal tilings

Following the establishment of the geometric conditions governing the design of the pentagonal tilings, the next step involves the transformation of these systems into chiral honeycombs. This was carried out through the generation of circular chiral nodes at the vertices of the tilings, which are connected together through tangentially-attached ligaments. Besides the original geometric parameters used to design the base tessellations, two new independent dimensions are introduced as a result of chiralisation [62]: the chiral node radius, r, and the ligament thickness, t (see Fig. 3). The ligament length, l, is defined as a function of these new parameters and the distance between vertices, R, which is equal to i, j or k depending on the pair of vertices involved, as follows:

$$l = 2\sqrt{\left(\frac{R}{2}\right)^2 - \left(r - \frac{t}{2}\right)^2} \tag{7}$$

The transformation of pentagonal tessellations into the corresponding chiral structures also entails the consideration of additional geometric conditions for the realisation of these systems. The first criterion is that the distance between the centre of the chiral nodes, R, must be greater than the sum of the radii of the two chiral nodes being connected ($2r$ in this case) in order for the system to have a ligament length which is greater than zero and avoid overlap of the chiral nodes. This condition is necessary for the realisation of any chiral system, regardless of the type of base tessellation used. A second condition is also required in the case of pentagonal concave systems where $\alpha < 0°$ (i.e. $\delta > 90°$) in order to avoid the design of systems with ligaments intersecting chiral nodes. This condition depends on the direction of chiralisation (clockwise or anti-clockwise), which is presented in more detail in the Discussion section later on. In this work, we employed clockwise chiralisation, which is subject to the following condition:

$$\cos\left[\arccos\left(\frac{2r - t}{k}\right) + \beta\right] < -\frac{t}{i} \tag{8}$$

Table 1
List of geometric parameters used.

Geometric parameters	
i	24 mm
j	$0.2(i)\ldots1.5(i)$ in steps of $0.1(i)$
k	$0.2(i)\ldots1.5(i)$ in steps of $0.1(i)$
r	1, 2, 3, 4, 5 mm
t	0.3 mm

3. Methodology

In order to explore the mechanical properties of these novel pentagonal tiling-based chiral metamaterials, we used the Finite Element Method (FEM) to conduct a parametric study and simulate the on-axis loading behaviour of a range of geometries. Following the parametric study, a more in-depth follow-up experimental and numerical analysis was conducted on three systems which are representative of a pentagonal chiral metamaterial exhibiting a highly positive, highly negative and zero Poisson's ratio separately. In the following sections, a detailed description of the methodology used is provided.

3.1. Parametric finite element analysis

As stated previously, initially, the Finite Element Method (FEM) was utilised to conduct a parametric study and simulate the on-axis loading behaviour of a range of geometries. For the design of the base tessellations, i was set to 24 mm, with the values of j and k varying from $0.2(i)$ to $1.5(i)$ in steps of $0.1(i)$ for each i value. In the case of the chiralisation geometric variables, for the initial parametric run, the chiral node radius, r, was varied from 1 mm to 5 mm in steps of 1 mm, while the parameter t was kept constant at 0.3 mm. The complete set of values used are specified in Table 1. Naturally, not all these combinations of parameters satisfy the conditions indicated in Appendix A necessary to yield realisable structures, and, therefore, the total number of simulations conducted was lower than the full factorial set. Following this wide-ranging analysis, additional simulations were also conducted using a more specific set of geometric parameters with variations at smaller intervals in order to investigate closely certain interesting characteristics observed following the preliminary screening of results, of which more details are provided in the Results and Discussion section.

The numerical simulations were conducted using the ANSYS16 Multiphysics software. In order to maximise computational efficacy, the systems were simulated as single representative unit cells (RUCs) subjected to periodic boundary conditions (PBCs). The geometries were meshed using the PLANE183 element (a higher-order 8-noded element with quadratic displacement behaviour and two degrees of freedom at each node) [75] using a minimum mesh size of $t/4$, which was chosen following mesh-size convergence testing. The constitutive material properties used were an isotropic Poisson's ratio of 0.3 and a Young's modulus of 200 GPa. PBCs were implemented through the use of constraint equations which are used to bind the displacements of paired nodes on the edges of the RUC. The system was fixed from a single point in space and the unit cell was constrained to remain globally aligned with the y-axis at all times throughout deformation. This simulation technique, which is described in detail in [76], has been validated and used in previous works to study systems possessing no axis of mirror symmetry. The structures were subjected to uniaxial loading in the x- and y-directions separately through the application of a unitary tensile force on the respective boundaries of the systems and solved linearly in order to obtain the Poisson's ratio and Young's modulus. Finally, in order to confirm the presence of transverse isotropy in these systems, we also conducted additional simulations on a representative set of structures where the shear modulus was measured and compared with the expected value which was obtained from the Poisson's ratio and Young's modulus; the results of which are presented in the Supplementary Information.

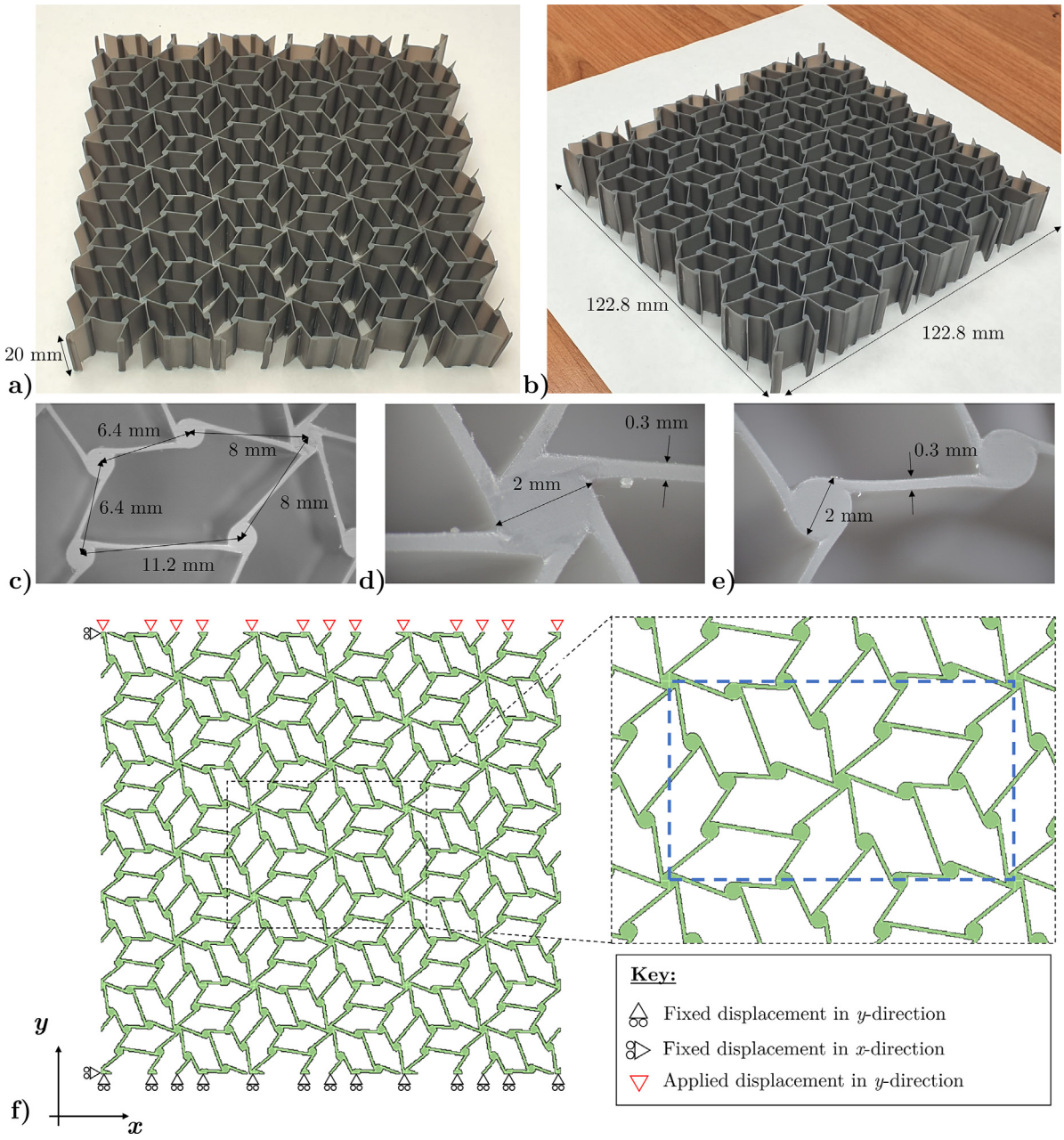

Fig. 4. (a–e) Images of Structure I from different angles and magnifications with measurements. (f) Diagram showing the loads applied on the finite planar system corresponding to Structure 1 (3 × 5 RUCs). The system was fixed in the y-direction from all the nodes on the bottom edge and in the x-direction from the one node only. Compressive strain was imposed through the application of a displacement on the topmost nodes in the y-direction. The Poisson's ratio was measured from the edges of the central RUC (marked in blue), similarly to the DIC analysis of the experimental prototypes. (For interpretation of the references to colour in this figure legend, the reader is referred to the web version of this article.)

3.2. Experimental tests and non-linear finite element simulations

In addition to the large set of linear simulations, non-linear simulations and experimental tests were conducted on three additively manufactured prototypes representative of these pentagonal tessellation-based chiral honeycombs (Structures I, II and III). The relative parameters of these three systems were chosen on the basis of the results obtained from the linear simulations, while the absolute values were dictated by the resolution and platform-size limits of the 3D printer, and presented in Table 2. Each of the three structures was designed as a planar 3 × 5 RUC system (i.e. containing 3 RUCs in the horizontal direction and 5 RUCs in the vertical) with an extruded depth of 20 mm using ANSYS16 Multiphysics and converted to STL files. This out-of-plane width is over 66 times the size of the in-plane ligament thickness and is sufficient to ensure that no out-of-plane deformation occurs during loading. One specimen of each of these structures was then additively manufactured using a Formlabs3® stereolithography 3D printer using the Formlabs® Tough 2000 Resin material [77] (see Fig. 4).

Table 2
Dimensions of the three additively manufactured prototypes. The parameter d represents the out-of-plane thickness or depth of the structures.

Structure	r/mm	t/mm	d/mm	i/mm	j/mm	k/mm	j/i	k/i
I	1.0	0.3	20	8.0	6.4	11.2	0.80	1.40
II	1.0	0.3	20	8.0	5.0	4.0	0.63	0.50
III	1.0	0.3	20	8.0	2.4	11.2	0.30	1.40

These three structures were subjected to *quasi*-static small-strain compressive loading tests using a Testometric Tensile loading machine

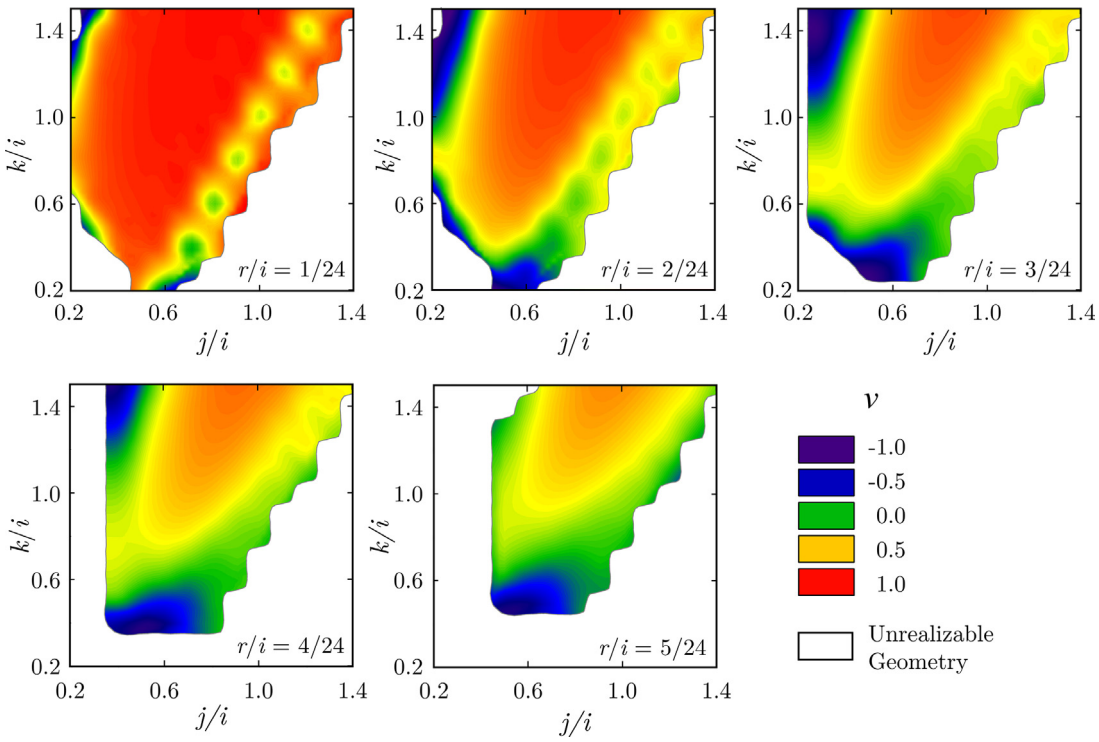

Fig. 5. Contour plots showing the range of Poisson's ratios which may be obtained for chiralised pentagonal tessellations with hexagonal symmetry with varying node radius, r, and pentagon side lengths, k/i and j/i. The parameter i for these systems was set at a constant value of 24 mm while the ligament thickness, t, was fixed at 0.3 mm. The full set of results, including Young's modulus data are presented in the Supplementary Information.

with a 50 Kgf loadcell (Serial No. 70197) at a speed of 5 mm/min. The Poisson's ratio of the central RUC of each system was measured through Digital Image Correlation (DIC) using a Messphysik videoextensiometry system. This was done by marking the corners of the central RUC and tracking the displacement of the marked points in order to calculate the strains of the overall RUC from which the Poisson's ratio may be calculated.

In addition to the experimental tests, non-linear geometric simulations were also run on corresponding finite systems equivalent to the three tested prototypes, i.e. under non-periodic simulation conditions. The simulations were conducted on plane models under plane-strain conditions and the system was loaded in a method analogous to the experiments as shown in Fig. 4f. The bottom surface was fixed in the y-direction and in the x-direction from one corner only, while the upper surface was fixed from one node only in the x-direction (in order to retain the alignment of the structure) and subjected to small compressive strains (of up to 5% globally) in the y-direction in small incremental steps. This results in a loading mode which is identical to that experienced by the experimental prototypes upon compressive loading. The Poisson's ratio was measured from the four corners of the central unit cell as in the experimental tests. Since the chiral structures were subjected primarily to strains which are well within the elongation limit of the base resin used, linear isotropic material properties were used for the simulations, with the Young's modulus being set to 1.68 GPa and the Poisson ratio to 0.45 [34].

4. Results and discussion

In this section the results obtained from the parametric Finite Element analysis and the experimental tests on the 3D-printed prototypes are presented and discussed separately. This is followed by a general discussion of all the findings obtained in this study which considers both sets of results together and draws the general conclusions of this work.

4.1. Linear finite element simulations

The results obtained for the Poisson's ratios of a representative set of the simulated systems are presented in Fig. 5. This set of results comprises systems with a fixed i value of 24 mm and t value of 0.3 mm, while the geometric parameters j, k and r are varied. The full set of results for the entire simulation run is presented in the Supplementary Information. As one can observe for Fig. 5, these chiralised pentagonal tessellations have the ability to exhibit a very wide range of Poisson's ratios which cover the full spectrum of 2D isotropy (+1 to −1). In numerical terms, the highest Poisson's ratio obtained was +0.986, while the lowest value was −0.983 (see Supplementary Information). This large versatility is present despite the geometric bounds described in the previous section which limit the range of realisable geometries. These geometric constraints are particularly pronounced in the case of highly chiralised systems (i.e. systems with large node radius to ligament length ratios); as illustrated in Fig. 5, where a wider range of geometries are allowed for systems with $r = 1$ mm than for structures with $r = 5$ mm. Moreover, it is evident that systems with small chiral node radii tend to exhibit predominantly high, positive Poisson's ratios, while systems with larger nodes typically possess lower values, including negative and zero Poisson's ratio values.

The contour plots indicate that certain pentagonal configurations have a high propensity to yield negative Poisson's ratios upon chiralisation. Specifically, pentagons with a combination of low j/i and k/i ratios have a particular affinity to exhibit auxetic behaviour, while the same applies to systems with a combination of low j/i and very high k/i ratios. The former cases, illustrated in the bottom left corner of Fig. 6a (an example of which is Structure A), comprise of systems which are made up of convex pentagons with two relatively long sides (both of length i) and three short sides (of length k and j). These systems deform predominantly through the rotation of the chiral nodes at the centre point axis of the six-fold rotational symmetry of the system and flexure of the ligaments with length i. A similar effect is also observed for the systems comprising of pentagons with low j/i and very high

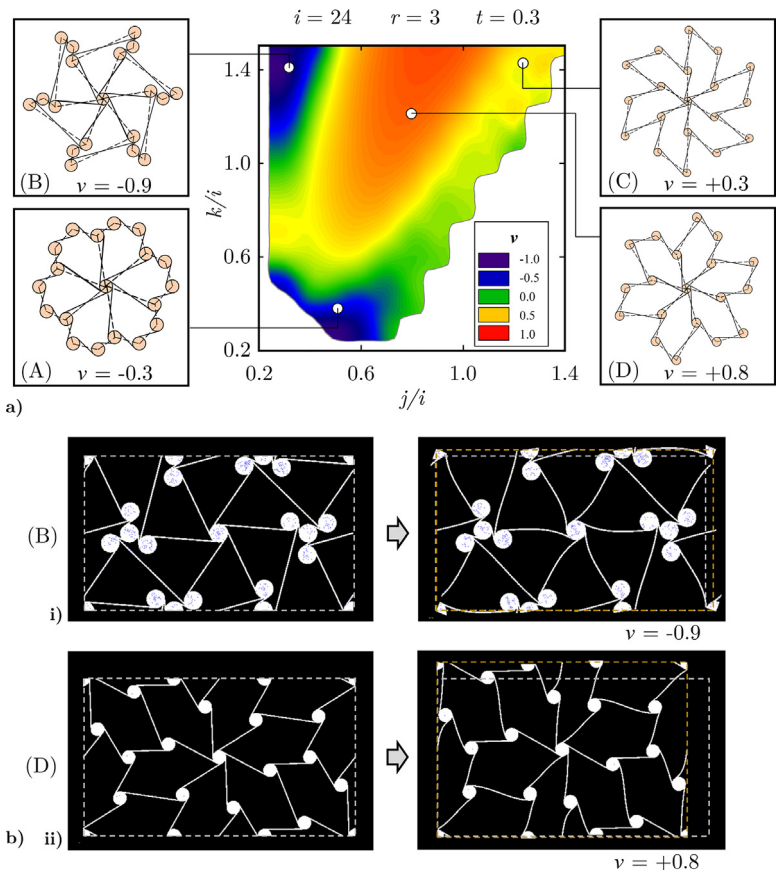

Fig. 6. (a) A pictorial representation of the range of chiralised monohedral pentagonal tessellations with hexagonal symmetry which may be obtained by varying the polygon side-length ratios. (b) Diagrams showing the deformed and undeformed states of two pentagonal tessellation-based chiral honeycombs (B) and (D) when subjected to uniaxial tensile loading in the vertical direction. (i) The first system, which has the following geometric parameters: $i = 24$ mm, $j/i = 0.3$, $k/i = 1.4$, $r = 3$ mm and $t = 0.3$ mm; possesses a Poisson's ratio of −0.9, while (ii) the second system: $i = 24$ mm, $j/i = 0.8$, $k/i = 1.2$, $r = 3$ mm and $t = 0.3$ mm; has a Poisson's ratio of +0.8. The images of the deformed structures were generated by magnified displacement scaling of the results obtained from the linear solution in order to allow for better observation of the deformation mechanisms.

k/i ratios (Structure B shown in Fig. 6b(i)), although in this case there is also flexure of ligaments with length k. These systems consist of concave pentagons possessing a negative α angle (as shown in Fig. 2) and have an inherent propensity to exhibit auxetic behaviour. Due to the concavity of the monohedral base pentagon shape, there are strict geometric limits to the extent to which these systems may be chiralised. In fact, as shown in Fig. 5, concave systems which have a large node radius (i.e. $r/i = 5/24$) are not geometrically realisable and thus, only pentagonal tessellations with low k/i and j/i ratios can be used to design isotropic auxetic structures.

On the other hand, systems with high j/i and k/i ratios (such as the one shown in Fig. 6a: Structures C and D) tend to exhibit positive Poisson's ratios even in cases where the chiral node radius is relatively large. This indicates that even upon the introduction of chiral geometric characteristics in these pentagonal tessellations, rotation of chiral nodes and symmetric S-shaped flexure of ligaments throughout the system (the hallmarks of the 'rotating chiral mechanism') are still not the main deformation modes. In fact, as shown in Fig. 6b(i), the deformation is characterised by a two-fold rotational symmetry rather than hexagonal rotation symmetry and may be described in terms of localised flexure of ligaments with minimal or no rotation whatsoever of chiral nodes. This deformation mode typically results in a positive Poisson's ratio and has been observed in other chiral systems which also do not exhibit auxetic behaviour [63].

In terms of the effective Young's modulus of these structures, E^*, there is also a great deal of variation in the values obtained. This value, which is calculated by taking the metamaterial Young's modulus and dividing it with that of the base material (in this case 200 GPa), gives a Young's modulus value which is characteristic of the geometric configuration only. As shown in Fig. 7, these structures have relatively low effective Young's moduli in comparison to that of the original material, with the highest values being at least four orders of magnitude lower. The spectrum of effective Young's moduli obtained ranges from 10^{-4} to 10^{-6} which is quite wide, but the relatively low values mean that these chiral metamaterials are primarily well-suited for the design of soft deformable systems such as flexible electronic circuits [78], robotic joints [79] and skin grafts [23] rather than load-resistant structures. Similarly to other chiralised 2D Euclidean tessellations [62,63], the Young's modulus of these systems generally decreases as the node radius increases, with the chiral honeycombs with $r = 5$ mm showing significantly lower values in comparison to those with $r = 1$ mm. Furthermore, it is evident that the systems possessing a negative Poisson's ratio are typically characterised by a relatively higher level of stiffness in comparison to those exhibiting a positive value for systems with the same node radii and ligament thicknesses. In particular, a trend is visible from Fig. 7 and the data listed in the Supplementary Information, showing that systems with a high k/i and low j/i ratios (concave systems with $\alpha < 0°$) and a low k/i and low j/i ratios exhibit the highest relative stiffness values for both barely and highly chiralised systems (i.e. low and high r/i ratio).

It is evident from the results obtained that the shape of the pentagons making up the monohedral tessellations is one of the main factors which determines the mechanical properties of these systems, including which structures have the ability to exhibit a negative or positive Poisson's ratio. However, as shown in Fig. 5, the extent of chiralisation also plays a very important role. It is clear that while certain pentagonal configurations have an inherent propensity to exhibit auxetic behaviour while others do not, overall, the Poisson's ratios of

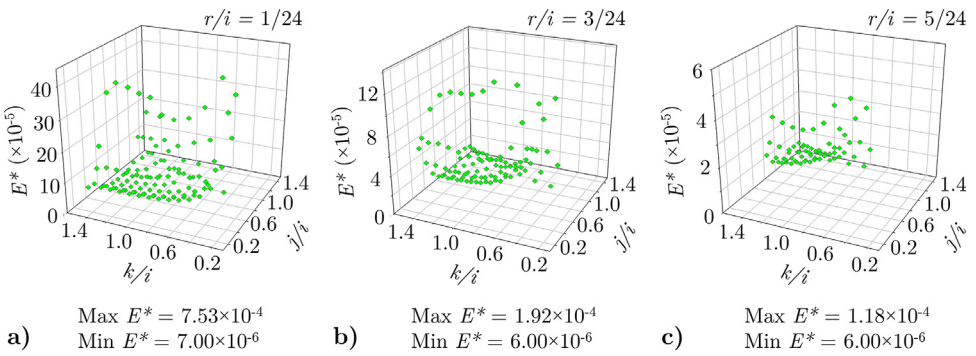

Fig. 7. 3D plots showing the changes in effective Young's modulus, E^*, for systems with $i = 24$ and $t = 0.3$, with three values of chiral node radii, $r = 1$, 3 and 5. The effective Young's modulus, E^*, is calculated as a ratio of the metamaterial Young's modulus and the base material Young's modulus ($E_{mat} = 200{,}000$ MPa). The maximum and minimum E^* values obtained for each set of structures is also indicated. The raw data for these graphs may be found in tabular form in the Supplementary Information.

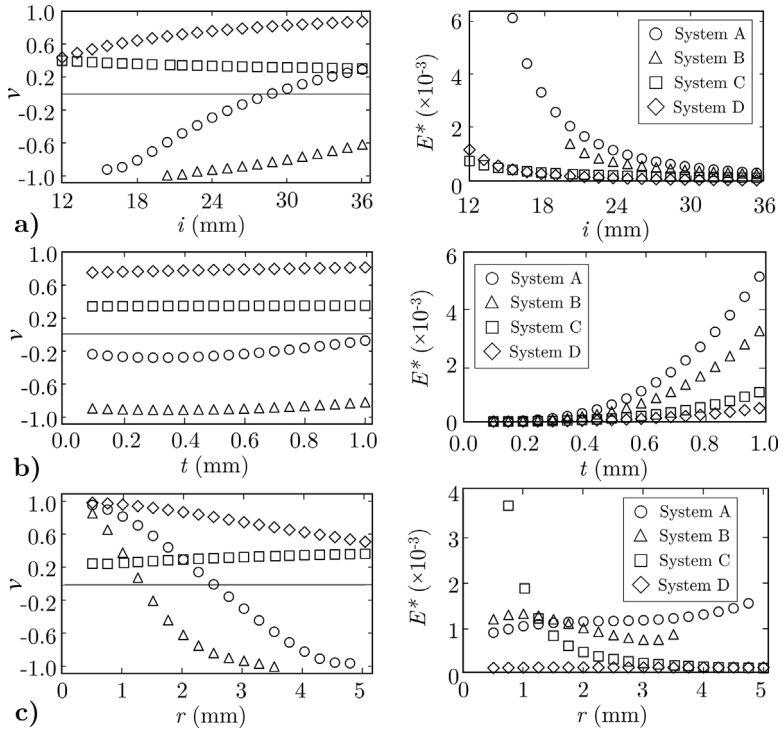

Fig. 8. Plots showing the variation in Poisson's ratio and Young's modulus for four systems upon changing the chiral geometric parameters (a) i, (b) t and (c) r separately. The missing values for Systems A and B in (a) and (c) are due to unrealisable geometries. For the graphs in (a), t and r were fixed at 0.3 and 3.0 mm respectively, while i was varied from 12 to 36 mm in steps of 1.2 mm. For (b) r and i were set to 3.0 and 24 mm respectively while t was varied from 0.1 to 1.0 mm in steps of 0.05 and finally, for (c), t and i were fixed at 0.3 and 24 mm respectively while r was varied from 0.5 to 5 mm in steps of 0.25 mm.

the entire range of pentagonal systems generally decreases as the extent of chiralisation increases. The extent of chiralisation can be quantified in terms of three geometric parameters: the ligament lengths, the node radii and the ligament thickness. Of these three parameters, two are listed as the independent variables r and t, while the ligament lengths, which are dependent on the dimensions of the pentagons can be calculated from Eq. (7). In order to quantitatively analyse the effect of these parameters on the mechanical properties of these chiral systems, a further set of structures was analysed where the parameters j/i and k/i were kept constant while the parameters i, t and r were varied individually. Four pentagonal shapes were chosen, represented by the four figures indicated in Fig. 6a, possessing the following parameters (shown in Table 3):

The results of these additional simulations are presented in Fig. 8, where the parameters i, t and r are varied separately whilst keeping all other parameters constant. It is evident from the plots that these parameters influence the mechanical properties of pentagonal chiral tessellations in different ways. For instance, an increase in the parameter i, which determines the size of the skeleton pentagonal tessellation with respect to the chiral node radius and ligament thickness, is shown to generally result in an increase in the Poisson's ratio. As demonstrated in Fig. 8a, this is the case for Systems A, B and D, but not for C, where the Poisson's ratio remains more or less unchanged and shows only a slight drop in magnitude upon increasing the value of i. In the cases of Systems A, B and D, the effect of this parameter is more

Table 3
Relative geometric parameters of the four pentagonal tessellations chosen for further studies (shown in Fig. 9).

System	j/i	k/i
A	0.5	0.4
B	0.3	1.4
C	1.2	1.4
D	0.8	1.2

pronounced, particularly in the case of System A, where the Poisson's ratio varies from −0.9 for the system with $i = 12$ mm all the way to +0.2 for the system with $i = 36$ mm. For Systems B and D, the increase in Poisson's ratio is smaller in magnitude but still significant. These trends are in accordance with those observed in previous studies on chiralised 2D tessellations, where a decrease in the node radius to ligament length ratio, and hence a decrease in chiralisation, results in an increase in the Poisson's ratio. The results for the effective Young's modulus upon changing i are more uniform in terms of trends; the stiffness decreases upon increasing the magnitude of i. This tendency is congruent with expectations derived from standard beam theory since increasing ligament length whilst retaining a constant cross-sectional thickness is known to result in a lowering of the flexural stiffness. The fact that Systems A and B possess the highest level of stiffness at low i values and show the greatest variation of effective Young's modulus upon changing i can also be explained by the fact that these systems possess extremely short ligaments in geometries with low i values (i.e. possessing ligament length to thickness ratios lower than 10) and thus the effects of mixed shear/flexure deformation modes result in these systems being relatively stiff in comparison to corresponding Systems C and D.

In terms of ligament thickness, t, the plots in Fig. 8b, indicate that this parameter has minimal effect on the Poisson ratio of these systems. In fact, only a small increase is observed in the Poisson's ratio of all four systems upon increasing the thickness of the ligaments. On the other hand, it is evident that ligament thickness has an extremely large influence on the stiffness, especially in the case of the auxetic systems (Systems A and B), where an exponential increase in effective Young's modulus is observed upon increasing the ligament thickness. This observation can also be attributed to beam theory since it is common knowledge that the stiffness of ligament-based structures increases upon increasing the cross-sectional thickness of the beam [80] and the systems presented here deform primarily through flexure/bending. This outcome is extremely useful since it indicates that it is possible to optimise and control the stiffness of these systems without considerably altering the Poisson's ratio of these metamaterials merely through an adjustment of the parameter t.

Finally, the results for varying the chiral node radius, r, presented in Fig. 8c, give rise to a number of points of interest. It is immediately clear that, unlike the previous two sets of results, there is no general trend which may be observed for the four systems. Furthermore, one can easily notice that variations of this parameter have a very pronounced effect on the Poisson's ratio of these systems which eclipses that observed for changing the parameters i or t. For Systems A and B, for instance, the Poisson's ratio varies from +0.98 for the geometry with $r = 0.5$ mm, all the way to −0.96 for structures with larger r values. This encompasses the entire range of the limits for 2D isotropy in terms of Poisson's ratio and shows how an increase in chiralisation, brought about by an increase in r, may be used to convert tessellations with high positive Poisson's ratios into auxetic metamaterials without any variation in rotational symmetry. In the case of System D, an increase in r is not sufficient to bring about a change in the sign of the Poisson's ratio, however, the Poisson's ratio still drops considerably from +0.99 to *ca.* +0.5 upon changing the value of r from 0.5 to 5 mm. On the other hand, in the case of System C, the opposite trend is observed; i.e. the Poisson's ratio marginally increases from +0.2 to +0.4 upon increasing the value of r by the same extent. This small change is not however, mirrored in the plots for the effective Young's modulus. Indeed, it is evident that System C is the most highly affected in terms of changes in stiffness with respect to variations in node radius out of the four pentagonal tessellations, where, as shown in Fig. 8c, the Young's modulus plummets exponentially upon increasing the value of r. Conversely, System D exhibits almost no changes in the effective Young's modulus upon increasing the node radius, with only a very minor increase in stiffness observed. Finally, even the two systems with a propensity to exhibit auxetic behaviour, Systems A and B, show contrasting trends. Whilst for System A, the effective Young's modulus generally increases upon increasing the node radius, the opposite is observed for System B, where the stiffness decreases. These findings highlight the diverse ways in which chiralisation influences the mechanical properties of these pentagonal tessellation-based metamaterials, with the variations in tendencies and extent of changes underlining the versatility of this method for designing isotropic systems with tailorable mechanical properties.

4.2. Experimental and finite non-linear simulations

In order to validate the FEM simulations and verify the findings presented in the previous section, experimental testing was conducted on three representative pentagonal-tessellation-based chiral systems produced through additive manufacturing. These three structures were chosen on the basis of the FEM simulations with the aim of demonstrating the full range of Poisson's ratios of this class of metamaterials. Hence, the constructed systems, shown in Fig. 9a and denoted as Structures I, II and III, are capable of exhibiting positive, zero and negative Poisson's ratios respectively. In addition to the experimental compressive tests on these systems, equivalent simulations were conducted on corresponding finite systems (shown in Fig. 9c) and infinite, periodic systems under non-linear geometric high-strain loading conditions as described in the methodology section.

The plots in Fig. 9d show that the results obtained from the experimental tests are extremely close to those extracted from both sets of FEM simulations. The similarity in deformation modes can also be visually observed from Fig. 9b and c (videos are also presented in the Supplementary Information), where the deformed state of each structure at *ca.* 2.5% compressive strain is shown. As predicted by the initial linear simulations, Structure I exhibits a highly positive Poisson's ratio of +0.82, which is retained over the entirety of the applied strain range while, conversely, Structure III shows a highly negative Poisson's ratio of −0.74 which also remains constant. Structure II, on the other hand, shows an initial low positive Poisson's ratio of ca. +0.1, which gradually decreases upon increasing the strain until it reaches almost −0.1 at 2.5% compressive strain. This indicates that it has a Poisson's ratio which is close to zero at these small strains, which, however, is not retained at higher strains, at which the system starts to gradually exhibit small auxetic behaviour. The plots also show that there is significant congruency between the experimental and simulations, which is particularly evident in the case of Structure I, where the plots of the FEM results and experimental data are almost superimposed on top of each other. For Structure II, the numerical simulations both predict an initial Poisson's ratio of quasi zero, which gradually evolves to small negative values at higher strains similar to the experimental results. This result indicates that the zero Poisson's ratio of these systems is not expected to be retained for high strains. In the case of Structure III, the differences between simulations and experimental results are slightly more pronounced, with the Poisson's ratio of the experimental prototype (−0.74) being less negative than the FEM predictions (−0.82 and −0.86 for the finite and infinite systems respectively). This difference is most probably due to the presence of defects in the prototype related to the printing of very small ligaments, which are not present in Structures I and II. However, despite this small difference in magnitude, the trends observed are identical. At this point, it is also important to highlight that the congruency between the finite simulations and experimental results with the periodic simulations for each of the three structures indicates that, despite the relatively small number of RUCs in the former two systems, the influence of edge effects appears to be minimal and that the deformation mechanisms of the central unit cell of these metamaterials are not greatly affected by boundary factors.

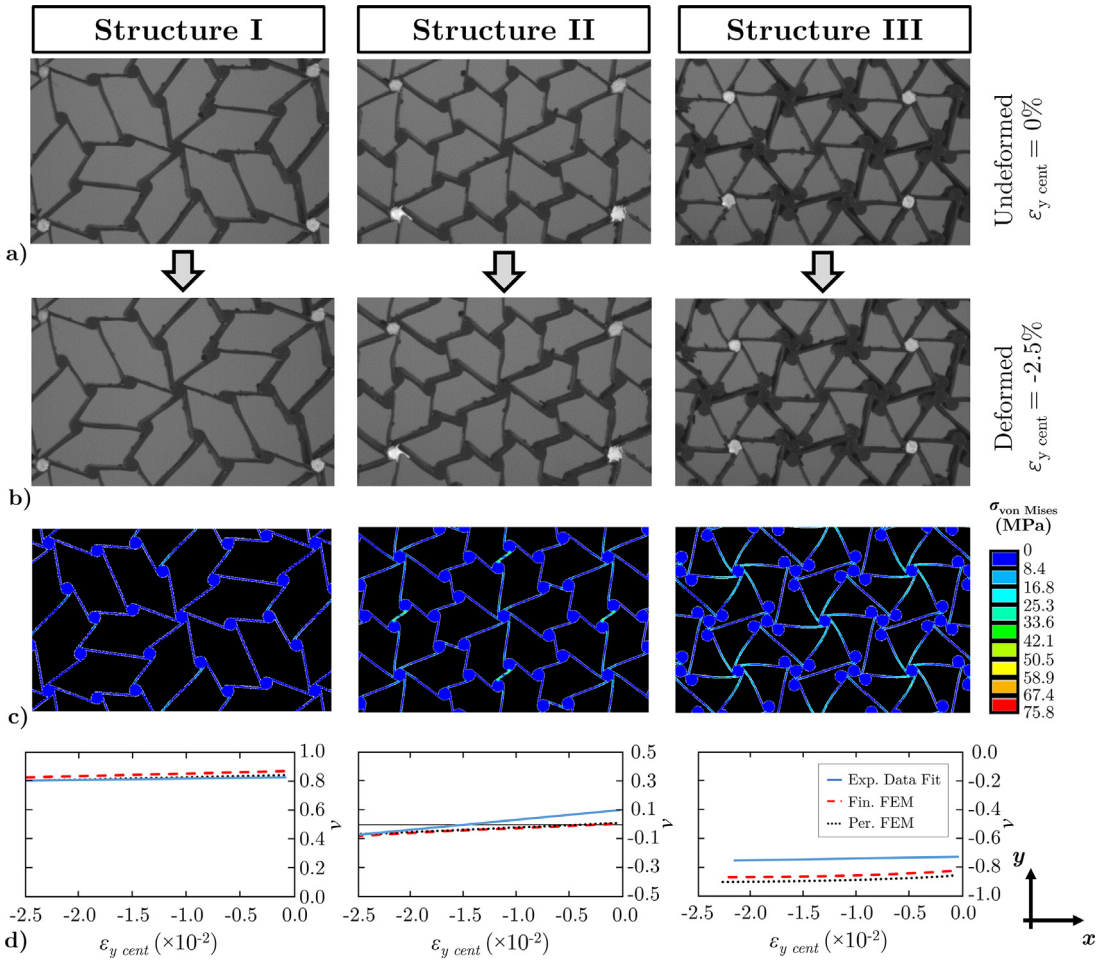

Fig. 9. Images showing the (a) undeformed and (b) deformed experimental prototypes (Structures I, II and III) subjected to *ca.* 2.5% compressive engineering strain of the central unit cell in the *y*-direction (ϵ_{ycent}). The white spots indicate the markers at the corner of the RUC from which the Poisson's ratio of the central cell was measured using DIC. Image set (c) shows the corresponding FEM simulations on finite equivalents of the 3D-printed prototypes and the elastic von Mises stress distribution obtained, while the plots in (d) show a comparison of the engineering Poisson's ratios measured from the experimental, finite FEM and periodic FEM geometric nonlinear simulations, plotted with respect to engineering strain applied on the central RUC (ϵ_{ycent}). Videos showing the full deformation of the experimental and FEM simulations are provided in the Supplementary Information. The raw data pertaining to the strain measurements of the experimental systems are also presented in the Supplementary Information.

4.3. Discussion and outlook

The findings of this study clearly demonstrate that chiral honeycombs based on monohedral pentagonal tessellations are a promising new class of mechanical metamaterials and have the potential to exhibit a wide range of geometrically-tailorable mechanical properties whilst retaining their transverse isotropy. The latter property arises from the fact that these systems retain their hexagonal rotational symmetry even when the geometric parameters which govern their deformation behaviour and mechanical properties are altered. The Poisson's ratio of these systems encompasses the entire range permissible by two-dimensional isotropy and is determined primarily by tessellation shape and extent of chiralisation. An analysis of the trends observed from Fig. 5 indicates that in order to produce auxetic chiral pentagonal systems, one should generally stick to the following main design specifications:

I. Increasing the extent of chiralisation (i.e. increase in node radius, *r*, relative to ligament thickness, *t*, and ligament length, *l*) generally results in a lower, more negative Poisson's ratio.
II. Designing the chiral systems on the basis of pentagonal tessellations with a low *j*/*i* ratio AND a very low *k*/*i* ratio OR a very high *k*/*i* ratio typically yields systems with highly negative Poisson's ratios

On the other hand, in order to produce systems with a highly positive Poisson's ratio, then one should do the opposite by decreasing the extent of chiralisation and choosing a base pentagonal tessellation which has a large or intermediate *k*/*i* ratio and an intermediate *j*/*i* ratio.

The effective elastic modulus of these systems also shows significant versatility and can also be tailored according to geometry. This extent of permissible variation in mechanical properties is not widely present in currently known isotropic metamaterials, where the number of changeable variables is typically extremely limited due to the imposed symmetry constraints. In this regard, chiralised pentagonal tessellations are decidedly superior to other well-known isotropic metamaterials such as hexachiral and trichiral honeycombs, since they have a far larger range of geometric parameters which may be altered according to the desired design specifications. Furthermore, it should be noted that these isotropic chiral metamaterials are generally characterised by a higher effective Young's modulus in comparison to anisotropic chiral metamaterials based on quadratic symmetry such as tetrachiral and anti-tetrachiral honeycombs which are typically extremely weak to loading in non-orthogonal directions.

Another important aspect of these systems which merits mention is the "direction" of chiralisation of these systems and its effect on mechanical properties. Chiral honeycombs are always characterised by a specific direction in which the ligaments are oriented with respect to nodes, which can be described as 'clockwise' or 'anti-clockwise' as shown in Fig. 10. Generally, this factor is not considered important

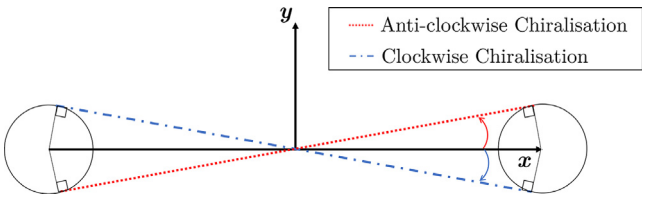

Fig. 10. A schematic showing how clockwise and anti-clockwise chiralisation may be defined. In this work, all systems were chiralised in a clockwise direction.

since it only determines the direction in which the chiral nodes rotate upon the application of a load and has no influence on the mechanical properties of the metamaterial. This statement holds true for chiral systems based on regular monohedral tessellations such as hexachiral, tetrachiral and trichiral honeycombs as well as many 2D Euclidean polyhedral tessellation-based chiral systems due to the fact that the original base tessellations of these chiral systems are characterised by multiple axes of mirror symmetry. This means that, consequently, once these tessellations are 'converted' into chiral metamaterials, the resultant structures formed by clockwise and anti-clockwise chiralisation are mirror-images of each other and, thus, 'identical' from a mechanical standpoint. However, the pentagonal tessellations which form the basis of these novel chiral honeycombs presented in this work, originally have no axes of mirror symmetry and are characterised by rotational symmetry only. This means that, in terms of symmetry, these tessellations are 'left' or 'right'-handed before being chiralised and, therefore, the resultant structures formed by chiralising in a clockwise and anti-clockwise direction are not congruent, but unique. Thus, it follows, that systems formed by clockwise and anti-clockwise chiralisation should have different mechanical properties. This indicates that further to the geometric parameters considered in this work, another additional parameter exists which could be used to further increase the versatility of these systems; namely, the direction of chiralisation. In this work, all of the systems studied were chiralised in a clockwise direction and, although preliminary investigations indicate that, for anti-clockwise chiralisation, the general trends for the design of auxetic structures listed previously are still expected to hold, the magnitudes of the Poisson's ratios and Young's moduli are predicted to be different. Further studies are required in order to fully investigate the effect of this factor on the mechanical properties of this novel class of chiral honeycombs.

This work also highlights the potential of 2D monohedral pentagonal tessellations for the design of novel auxetic metamaterials. Pentagon-based structures have traditionally been overlooked as candidates for the design of auxetic systems; a factor which may be primarily attributed to the fact that regular pentagons cannot form periodic lattices. However, as mentioned previously in the Concept and Design section, irregular pentagons can form a variety of distinct periodic tessellations with a diverse range of symmetry properties. Although only the one investigated in this work shows hexagonal rotational symmetry and, hence, only it is capable of exhibiting transverse isotropy, the other systems are promising candidates for the design of new anisotropic auxetic metamaterials through chiralisation. Indeed, one of these additional systems has already been shown in a separate study to have the potential to exhibit auxeticity as a ligament-based tessellation [81] *per se*, without chiralisation, while other works have also shown that pentagon-based tessellations may form the basis of the theoretical "penta-graphene" [82,83] 2D crystal lattice structure. Moreover, another important research aspect which should be explored in the near future, concerns the high strain behaviour of these systems. While this study was focused primarily on the linear behaviour of these novel chiral tessellation, further research is necessary to determine the extent to which these systems retain their mechanical properties under high stress/strain conditions as well as the fatigue limits and fracture mechanics of these metamaterials. All this indicates that there are many potential advances and avenues for further research in this promising and relatively unexplored class of monohedral pentagonal Euclidean tessellations.

5. Conclusion

In this work, a novel class of isotropic 2D mechanical metamaterials is proposed and investigated. These metamaterials, which have the ability to exhibit Poisson's ratios which encompass the entire spectrum of transverse-isotropicity, are designed through the chiralisation of a special class of monohedral irregular pentagonal tessellations which possess rotational symmetry of order 6. The influence of various geometric parameters, including base tessellation dimensions, chiral node radius and ligament thickness on the mechanical properties of these systems were investigated using the FEM. Furthermore, experimental tests on additively-manufactured prototypes were conducted to validate the FEM results obtained, while analytical expressions which may be used to determine which combination of geometric parameters yields realisable chiral structures were also derived. The main findings of this work may be summarised as follows:

- The Poisson's ratio and Young's modulus can be tailored as a function of the geometric parameters of these systems whilst retaining isotropy.
- These new chiral metamaterials have the ability to exhibit Poisson's ratios ranging from −1 to +1.
- The Young's modulus of these systems is also highly tuneable and shows considerable variation.
- In some cases, the Young's modulus can be altered without significantly affecting the value of the Poisson's ratio.
- Experimental testing on stereolithography-printed prototypes have confirmed the functionality of these systems

This work demonstrates that the retention of global symmetry and geometric constraints of isotropy are not necessarily a barrier for the design of geometrically-tailorable isotropic metamaterials and highlights the vast potential of pentagonal structures as the basis for the design of further new auxetic systems.

CRediT authorship contribution statement

Luke Mizzi: Writing – original draft, Software, Methodology, Investigation, Formal analysis, Conceptualization. **Luigi Grasselli:** Writing – review & editing, Validation, Methodology, Investigation, Formal analysis, Conceptualization. **Andrea Spaggiari:** Writing – review & editing, Validation, Methodology, Conceptualization. **Ruben Gatt:** Writing – review & editing, Resources, Investigation. **Pierre-Sandre Farrugia:** Writing – review & editing, Investigation. **Joseph N. Grima:** Writing – review & editing, Resources.

Declaration of competing interest

The authors declare that they have no known competing financial interests or personal relationships that could have appeared to influence the work reported in this paper.

Data availability

The raw data is available in the Supplementary Information

Appendix A. Geometric conditions for the design of pentagonal tessellations with hexagonal rotational symmetry

The conditions necessary for the design of pentagonal tessellation with hexagonal rotational symmetry and for the realisation of convex pentagons may be summarised by the equations presented below. The existence and convexity conditions are expressed as functions of $\frac{j}{i}$ and $\frac{k}{i}$ and are plotted in Fig. 2b. While the existence conditions (Eqs. (A.1), (A.2) and (A.3)) are inequalities directly derived from Eq. (1) in the main text, the convexity conditions (Eqs. (A.4), (A.5) and (A.6)) for angles β, γ and δ which must be satisfied for the design of tessellations made from convex pentagons are derived from Eqs. (4), (5) and (6).

Existence Conditions

$$\frac{j}{i}\sqrt{3}-\frac{k}{i}+1>0 \tag{A.1}$$

$$\frac{j}{i}\sqrt{3}+\frac{k}{i}-1>0 \tag{A.2}$$

$$\frac{j}{i}\sqrt{3}-\frac{k}{i}-1<0 \tag{A.3}$$

Convexity Conditions

$$\beta<120^\circ \qquad 3\left(\frac{j}{i}\right)^2-\left(\frac{k}{i}\right)^2-\left(\frac{k}{i}\right)-1<0 \tag{A.4}$$

$$\gamma<150^\circ \qquad 3\left(\frac{j}{i}\right)^2+\left(\frac{k}{i}\right)^2+3\left(\frac{jk}{i^2}\right)-1>0 \tag{A.5}$$

$$\delta<90^\circ \qquad 3\left(\frac{j}{i}\right)^2-\left(\frac{k}{i}\right)^2+1>0 \tag{A.6}$$

The existence region shown in Fig. 2b consists of the area between the two parallel lines $-\left(\frac{j}{i}\right)\sqrt{3}+\left(\frac{k}{i}\right)+1=0$ and $-\left(\frac{j}{i}\right)\sqrt{3}+\left(\frac{k}{i}\right)-1=0$, limited on the lower left corner by the line $\left(\frac{j}{i}\right)\sqrt{3}+\left(\frac{k}{i}\right)-1=0$. The convexity region is defined by a suitable branch of the hyperbola $-\left(\frac{j}{i}\right)^2+\left(\frac{k}{i}\right)^2+\left(\frac{k}{i}\right)+1=0$ ($\beta=120^\circ$), a suitable branch of the hyperbola $3\left(\frac{j}{i}\right)^2-\left(\frac{k}{i}\right)^2+1=0$ ($\delta=90^\circ$) and by the "positive" area of the ellipse $3\left(\frac{j}{i}\right)^2+3\left(\frac{jk}{i^2}\right)+\left(\frac{k}{i}\right)^2-1=0$ ($\gamma=150^\circ$).

Appendix B. Supplementary data

Supplementary material related to this article can be found online at https://doi.org/10.1016/j.tws.2023.110739.

References

[1] K. Bertoldi, V. Vitelli, J. Christensen, M. Van Hecke, Flexible mechanical metamaterials, Nat. Rev. 2 (2017) 17066.
[2] Y.C. Lakes, R.S. Lee, T. Bersie, A. Wang, Extreme damping in composite materials with negative-stiffness inclusions, Nature 410 (2001) 565–567.
[3] R.H. Baughman, S. Stafstrom, C. Cui, S.O. Dantas, Materials with negative compressibilities in one or more dimensions, Science (80-.) 279 (1998) 1522–1524.
[4] M. Calleja, A.L. Goodwin, M.T. Dove, Origin of the colossal positive and negative thermal functional theory study, J. Phys.: Condens. Matter 20 (2008) 255226.
[5] K.E. Evans, M.A. Nkansah, I.J. Hutchinson, J.A. Rogers, Molecular network design, Nature 353 (1991) 124.
[6] R. Lakes, Foam structures with a negative Poisson's ratio, Science (80-.) 235 (1987) 1038–1040.
[7] C. Luo, et al., Design, manufacturing and applications of auxetic tubular structures : A review, Thin-Walled Struct. 163 (2021) 107682.
[8] I.G. Masters, K.E. Evans, Models for the elastic deformation of honeycombs, Compos. Struct. 35 (1996) 403–422.
[9] H. Wan, H. Ohtaki, S. Kotosaka, G. Hu, A study of negative poisson's ratios in auxetic honeycombs based on a large deflection model, Eur. J. Mech. A 23 (2004) 95–106.
[10] A. Bezazi, F. Scarpa, C. Remillat, A novel centresymmetric honeycomb composite structure, Compos. Struct. 71 (2005) 356–364.
[11] H. Lu, X. Wang, T. Chen, In-plane dynamics crushing of a combined auxetic honeycomb with negative Poisson's ratio and enhanced energy absorption, Thin-Walled Struct. 160 (2021) 107366.
[12] J.N. Grima, K.E. Evans, Auxetic behavior from rotating squares, J. Mater. Sci. Lett. 19 (2000) 1563–1565.
[13] J.N. Grima, K.E. Evans, Auxetic behavior from rotating triangles, J. Mater. Sci. 1 (2006) 3193–3196.
[14] Y. Suzuki, et al., Self-assembly of coherently dynamic, auxetic, two-dimensional protein crystals, Nature 533 (2016) 369–373.
[15] L. Mizzi, E. Salvati, A. Spaggiari, J. Tan, A.M. Korsunsky, 2D auxetic metamaterials with tuneable micro-/nanoscale apertures, Appl. Mater. Today 20 (2020) 100780.
[16] K.K. Dudek, J.A. Iglesias Martinez, G. Ulliac, M. Kadic, Micro-scale auxetic hierarchical mechanical metamaterials for shape morphing, Adv. Mater. 34 (2022) 2110115.
[17] K.W. Wojciechowski, A.C. Branka, Negative Poisson ratio in a two-dimensional 'isotropic' solid, Phys. Rev. A 40 (1989) 7222–7225.
[18] D. Prall, R.S. Lakes, Properties of a chiral honeycomb with a Poisson's ratio of -1, Int. J. Mech. Sci. 39 (1997) 305–314.
[19] L. Mizzi, D. Attard, R. Gatt, P. Farrugia, J.N. Grima, An analytical and finite element study on the mechanical properties of irregular hexachiral honeycombs, Smart Mater. Struct. 27 (2018) 105016.
[20] L. Mizzi, et al., Influence of translational disorder on the mechanical properties of hexachiral honeycomb systems, Composites B 80 (2015) 84–91.
[21] A. Bacigalupo, L. Gambarotta, Simplified modelling of chiral lattice materials with local resonators, Int. J. Solids Struct. 83 (2016) 126–141.
[22] J. Shim, et al., Harnessing instabilities for design of soft reconfigurable auxetic/chiral materials, Soft Matter 9 (2013) 8198–8202.
[23] L. Mizzi, K.M. Azzopardi, D. Attard, J.N. Grima, R. Gatt, Auxetic metamaterials exhibiting giant negative Poisson's ratios, Phys. Status Solidi - Rapid Res. Lett. 9 (2015) 425–430.
[24] L. Mizzi, A. Spaggiari, Lightweight mechanical metamaterials designed using hierarchical truss elements, Smart Mater. Struct. 29 (2020) 105036.
[25] F. Scarpa, et al., Elastic buckling of hexagonal chiral cell honeycombs, Composites A 38 (2007) 280–289.
[26] I. Fernandez-Corbaton, et al., New twists of 3D chiral metamaterials, Adv. Mater. 31 (2019) 1807742.
[27] A. Airoldi, P. Bettini, P. Panichelli, M.F. Oktem, G. Sala, Chiral topologies for composite morphing structures – Part I: Development of a chiral rib for deformable airfoils, Phys. Status Solidi Basic Res. 252 (2015) 1435–1445.
[28] D. Attard, P.S. Farrugia, R. Gatt, J.N. Grima, Starchirals – A novel class of auxetic hierarchal structures, Int. J. Mech. Sci. 179 (2020) 105631.
[29] O. Sigmund, S. Torquato, Design of smart composite materials using topology optimization, Smart Mater. Struct. 8 (1999) 365–379.
[30] A. Lorato, et al., The transverse elastic properties of chiral honeycombs, Compos. Sci. Technol. 70 (2010) 1057–1063.
[31] A. Alderson, et al., Elastic constants of 3-, 4- and 6-connected chiral and anti-chiral honeycombs subject to uniaxial in-plane loading, Compos. Sci. Technol. 70 (2010) 1042–1048.
[32] A. Alderson, K.L. Alderson, G. Chirima, N. Ravirala, K.M. Zied, The in-plane linear elastic constants and out-of-plane bending of 3-coordinated ligament and cylinder-ligament honeycombs, Compos. Sci. Technol. 70 (2010) 1034–1041.
[33] K.K. Dudek, New type of rotation of chiral mechanical metamaterials, Smart Mater. Struct. 29 (2020) 115027.
[34] L. Mizzi, et al., Mechanical metamaterials with star-shaped pores exhibiting negative and zero Poisson's ratio, Mater. Des. 146 (2018) 28–37.
[35] W. Wu, et al., Mechanical design and multifunctional applications of chiral mechanical metamaterials: A review, Mater. Des. 180 (2019) 107950.
[36] Y. Niu, J. Ge, J. Liang, H. Liao, W. Wu, Effects of disordered circular nodes dispersion and missing ligaments on the mechanical properties of chiral structures, Phys. Status Solidi 256 (2019) 1–12.
[37] J.L. Silverberg, et al., Using origami design principles to fold reprogrammable mechanical metamaterials, Science (80-.) 345 (2014) 647–650.
[38] M. Schenk, S.D. Guest, Geometry of Miura-folded metamaterials, Proc. Natl. Acad. Sci. 110 (2013) 3276–3281.
[39] L. Rothenburg, A.A. Berlin, R.J. Bathurst, Microstructure of isotropic materials with a negative Poisson's ratio, Nature 354 (1991) 470–472.
[40] M.R. Sloan, J.R. Wright, K.E. Evans, Mechanics of Materials The helical auxetic yarn – A novel structure for composites and textiles ; geometry, manufacture and mechanical properties, Mech. Mater. 43 (2011) 476–486.
[41] W.T. Kelvin, Baltimore lectures on molecular dynamics and the wave theory of light, 1904.
[42] K.W. Wojciechowski, Two-dimensional isotropic system with a negative Poisson ratio, Phys. Lett. A 137 (1989) 60–64.
[43] W. Miller, C.W. Smith, F. Scarpa, K.E. Evans, Flatwise buckling optimization of hexachiral and tetrachiral honeycombs, Compos. Sci. Technol. 70 (2010) 1049–1056.
[44] H. Abramovitch, et al., Smart tetrachiral and hexachiral honeycomb: Sensing and impact detection, Compos. Sci. Technol. 70 (2010) 1072–1079.
[45] G. Cicala, et al., Hexachiral truss-core with twisted hemp yarns: Out-of-plane shear properties, Compos. Struct. 94 (2012) 3556–3562.
[46] A. Bacigalupo, L. Gambarotta, Homogenization of periodic hexa- and tetrachiral cellular solids, Compos. Struct. 116 (2014) 461–476.

[47] Y. Chen, X.N. Liu, G.K. Hu, Q.P. Sun, Q.S. Zheng, Micropolar continuum modelling of bi-dimensional tetrachiral lattices, Proc. R. Soc. A Math. Phys. Eng. Sci. 470 (2014) 20130734.
[48] R. Zhong, M. Fu, Q. Yin, O. Xu, L. Hu, Special characteristics of tetrachiral honeycombs under large deformation, Int. J. Solids Struct. 169 (2019) 166–176.
[49] X. Shiyin, H. Xiuchang, H. Hongxing, A study on the isolation performance of trichiral lattices with gradient geometry, JVC/J. Vib. Control 21 (2015) 3465–3475.
[50] L. Mizzi, E. Salvati, A. Spaggiari, J. Tan, A.M. Korsunsky, Highly stretchable two-dimensional auxetic metamaterial sheets fabricated via direct-laser cutting, Int. J. Mech. Sci. 167 (2020) 105242.
[51] Y.J. Chen, F. Scarpa, y. Liu, J.S. Leng, Elasticity of anti-tetrachiral anisotropic lattices, Int. J. Solids Struct. 50 (2013) 996–1004.
[52] R. Gatt, et al., A realistic generic model for anti-tetrachiral systems, Phys. Status Solidi b 250 (2013) 2012–2019.
[53] R. Gatt, J.P. Brincat, K.M. Azzopardi, L. Mizzi, J.N. Grima, On the effect of the mode of connection between the node and the ligaments in anti-tetrachiral systems, Adv. Eng. Mater. 17 (2015) 189–198.
[54] W. Wu, X. Song, J. Liang, Mechanical properties of anti-tetrachiral auxetic stents, Compos. Struct. 185 (2018) 381–392.
[55] A. Bacigalupo, M.L. De Bellis, Auxetic anti-tetrachiral materials: Equivalent elastic properties and frequency band-gaps, Compos. Struct. 131 (2015) 530–544.
[56] Y. Ma, et al., A nonlinear auxetic structural vibration damper with metal rubber particles, Smart Mater. Struct. 22 (2013).
[57] L. Mizzi, A. Sorrentino, A. Spaggiari, D. Castagnetti, A comparison between rotating squares and anti-tetrachiral systems : Influence of ligaments on the multi-axial mechanical response, Proc. Inst. Mech. Eng. C (2021) http://dx.doi.org/10.1177/09544062211043145.
[58] L.L. Hu, Z.J. Wu, M.H. Fu, Mechanical behavior of anti-trichiral honeycombs under lateral crushing, Int. J. Mech. Sci. 140 (2018) 537–546.
[59] L.L. Hu, W.K. Ye, Z.J. Wu, Mechanical property of anti-trichiral honeycombs under large deformation along the x-direction, Thin-Walled Struct. 145 (2019) 106415.
[60] J.N. Grima, R. Gatt, P.S. Farrugia, On the properties of auxetic meta-tetrachiral structures, Phys. Status Solidi Basic Res. 245 (2008) 511–520.
[61] P.-S. Farrugia, R. Gatt, L. Mizzi, J.N. Grima, Auxetic behavior obtained through the large deformations of variants of the rectangular grid, Mech. Adv. Mater. Struct. (2021) 1–10.
[62] L. Mizzi, A. Spaggiari, Chiralisation of Euclidean polygonal tessellations for the design of new auxetic metamaterials, Mech. Mater. 153 (2021) 103698.
[63] L. Mizzi, A. Spaggiari, Novel chiral honeycombs based on octahedral and dodecahedral Euclidean polygonal tessellations, Int. J. Solids Struct. 238 (2022) 111428.
[64] T. Tarnai, P.W. Fowler, S.D. Guest, Equiauxetic hinged archimedean tilings, Symmetry (Basel) 14 (2022) 1–15.
[65] D. Mousanezhad, et al., Elastic properties of chiral, anti-chiral, and hierarchical honeycombs: A simple energy-based approach, Theor. Appl. Mech. Lett. 6 (2016) 81–96.
[66] W. Wu, et al., Mechanical properties of hierarchical anti-tetrachiral metastructures, Extreme Mech. Lett. 16 (2017) 18–32.
[67] M. Fu, F. Liu, L. Hu, A novel category of 3D chiral material with negative Poisson's ratio, Compos. Sci. Technol. 160 (2018) 111–118.
[68] P. Farrugia, R. Gatt, J.N. Grima, A novel three-dimensional anti-tetrachiral honeycomb, Phys. Status Solidi 256 (2019) 1800473.
[69] S. Kuo, L. Shiau, K. Chen, Buckling analysis of shape memory alloy reinforced composite laminates, Compos. Struct. 90 (2009) 188–195.
[70] Y. Wei, Q. Yang, X. Liu, R. Tao, A novel 3D anti-tetrachiral structure with negative Poisson's ratio, Smart Mater. Struct. 29 (2020) 085003.
[71] T.C.T. Ting, T. Chen, Poisson's ratio for anisotropic elastic materials can have no bounds, Q. J. Mech. Appl. Math. 58 (2005) 73–82.
[72] E. Gao, R. Li, S. Fang, Q. Shao, R.H. Baughman, Bounds on the in-plane Poisson's ratios and the in-plane linear and area compressibilities for sheet crystals, J. Mech. Phys. Solids 152 (2021) 104409.
[73] B. Grünbaum, G.C. Shephard, Tillings and Patterns, second ed., Dover Publications, 2016.
[74] B. Grünbaum, G.C. Shephard, Tilings by regular polygons, Math. Mag. 50 (1977) 227–247.
[75] ANSYS16.
[76] L. Mizzi, et al., Implementation of periodic boundary conditions for loading of mechanical metamaterials and other complex geometric microstructures using finite element analysis, Eng. Comput. 37 (2021) 1765–1779.
[77] Formlabs, Engineering resin - tough 2000, 2022.
[78] B. Jang, et al., Auxetic meta-display: Stretchable display without image distortion, Adv. Funct. Mater. 32 (2022) 2113299.
[79] M. Kaur, W.S. Kim, Toward a smart compliant robotic gripper equipped with 3D-designed cellular, Adv. Intell. Syst. 1 (2019) 1900019.
[80] S. Timoschenko, J.N. Goodier, Theory of Elasticity, in: Engineering Societies Monographs, 1951.
[81] S. Winczewski, J. Rybicki, Negative Poisson's ratio from pentagons: A new auxetic structure combining three different auxetic mechanisms, Comput. Mater. Sci. 201 (2022) 110914.
[82] S. Zhang, et al., Penta-graphene: A new carbon allotrope, Proc. Natl. Acad. Sci. 112 (2015) 2372–2378.
[83] S. Winczewski, J. Rybicki, Anisotropic mechanical behavior and auxeticity of penta-graphene: Molecular statics/molecular dynamics studies, Carbon N. Y. 146 (2019) 572–587.